

# Variable-Frequency Phase Unwrapping for High-Speed 3-D Shape Measurement

Jinghui Zeng<sup>1</sup>, Yucheng Li<sup>1</sup>, Chen Xu<sup>1</sup>, Shutao Li<sup>2</sup>, *Fellow, IEEE*, and Mingkui Tan<sup>1</sup>, *Member, IEEE*

**Abstract**—Phase unwrapping plays a critical role in digital fringe projection (DFP) 3-D measurements. The phase unwrapping methods based on geometric constraints require no additional patterns, achieving superior efficiency and accuracy. However, our study reveals that existing methods suffer from a depth range imbalance (DRI) problem, leading to unwrapping failure and measurement error. This article presents a variable-frequency fringe pattern to address this problem. Unlike artificially defined constant-frequency fringes, we quantify the measurement depth range and theoretically determine the optimal fringe frequency according to the system parameters. Based on this, we propose a variable-frequency phase unwrapping (VFPU) method for high-speed 3-D shape measurement. The proposed method overcomes the DRI problem and maximizes the measurement accuracy and robustness. Extensive experimental results demonstrate the superiority of the proposed method in high-speed 3-D shape measurements.

**Index Terms**—3-D shape measurement, digital fringe projection (DFP), geometric constraint, phase unwrapping, variable frequency.

## I. INTRODUCTION

THE digital fringe projection (DFP) 3-D measurement technologies have been widely applied in industrial production and scientific research fields for the advantages of high precision, compact structure, and low cost [1], [2], [3]. DFP systems actively project structured fringe patterns and extract the phase information to recover the 3-D shape. However, the phase analysis algorithm can only provide the wrapped phase between  $-\pi$  and  $\pi$  with  $2\pi$  discontinuities, which

Manuscript received 28 April 2024; revised 20 July 2024; accepted 6 August 2024. Date of publication 26 August 2024; date of current version 18 September 2024. This work was supported in part by the National Natural Science Foundation of China (NSFC) under Grant 62072190, in part by the Key Realm Research and Development Program of Guangzhou under Grant 202007030007, and in part by the Program for Guangdong Introducing Innovative and Entrepreneurial Teams under Grant 2017ZT07X183. The Associate Editor coordinating the review process was Dr. Libing Bai. (Corresponding authors: Shutao Li; Mingkui Tan.)

Jinghui Zeng is with the Shien-Ming Wu School of Intelligent Engineering and the School of Software Engineering, South China University of Technology, Guangzhou 511442, China, and also with Pazhou Laboratory, Guangzhou 510335, China (e-mail: z.jh11@mail.scut.edu.cn).

Yucheng Li is with the College of Electrical and Information Engineering, Hunan University, Changsha 410082, China (e-mail: 707998032@qq.com).

Chen Xu is with Dongguan New Generation of Artificial Intelligence Technology Research Institute, Dongguan 523000, China (e-mail: xc.xc@qq.com).

Shutao Li is with the Greater Bay Area Institute for Innovation, Hunan University, Guangzhou 511300, China (e-mail: shutao\_li@hnu.edu.cn).

Mingkui Tan is with the School of Software Engineering and the Key Laboratory of Big Data and Intelligent Robot, Ministry of Education, South China University of Technology, Guangzhou 510006, China (e-mail: mingkuitan@scut.edu.cn).

Digital Object Identifier 10.1109/TIM.2024.3450114

affects unique phase matching [4], [5]. Therefore, the phase unwrapping technique that recovers the absolute phase has been one of the core procedures and gained a lot of research efforts in recent years [6], [7], [8], [9].

Classical phase unwrapping approaches can be mainly divided into two categories: the spatial phase unwrapping and the temporal phase unwrapping [6]. The spatial technologies assume the phase to be continuous, and recover the absolute phase by analyzing the adjacent phase values, including Goldstein's method [10], reliability-guided method [11], and Flynn's method [12]. These methods require no extra patterns and achieve high efficiency; however, it is challenging to handle complex surfaces with height jumps or occlusions. The temporal methods project additional patterns that can provide fringe order information [13], including the multifrequency phase-shifting method [14] and the Gray-code [15] method. These methods can be applied to complex surfaces and have higher robustness. However, acquiring extra fringe patterns severely reduces measurement efficiency [16]. To avoid extra fringe projections, researchers proposed to embed fringe order information into fringes [17], [18], [19], employ multiple cameras [20], or combine both [21], but such methods may degrade the phase quality or increase the hardware costs. In recent years, learning-based phase unwrapping methods have demonstrated promising performance [22], [23], [24]. However, the reliance on large amounts of training data limits their widespread application. Furthermore, incorporating physical priors to improve measurement stability and enhance interpretability remains to be further explored [25].

Different from these approaches, An et al. [26] proposed to employ the geometric constraints for phase unwrapping. By generating a virtual reference phase plane, the absolute phase can be recovered pixel-by-pixel. However, this method can only handle a phase range of  $2\pi$ , which means that the phase change caused by the object depth should not exceed  $2\pi$  with regard to the reference plane. Though decreasing the fringe frequency increases the depth range, the measurement accuracy would be affected [14], [27]. To overcome the depth range limitation, some studies focus on estimating the optimal reference planes. Jiang et al. [27] use prior knowledge to estimate multiple reference planes, and Dai et al. [28] use a known object to provide cues. However, it is challenging for these methods to flexibly measure unknown objects. Instead of artificially generating the reference plane, Wang et al. [29] adaptively evaluate the optimal reference plane according to the wrapped phase, but the measurement range is

still limited. On the other hand, some studies combine the geometric constraint with existing methods to increase the measurement range. Yu and Da [30] introduce the photometric information, but this method has specific requirements for the object surface's reflectivity. Tao et al. [31] propose to use multiple-camera constraints but increase the system complexity. The depth range can also be increased by combining with temporal methods, such as the two-frequency phase-shifting method [32], the Gray-code method [33], and the phase-coding method [34], however, sacrificing the measurement efficiency.

These related works based on geometric constraints mainly focus on expanding the measurement range and have made great progress. Estimating the depth range is critical for practical measurement since out-of-range causes incorrect results. However, to the best of our knowledge, the quantitatively calculating framework has not been established yet. Most existing methods treat the capture and projection lights as ideal parallel [26], [27], [35], ignoring the optical properties in which the light rays diverge from the optical center, that is, the pin-hole imaging model [36]. Moreover, existing analyses employ 1-D trigonometric derivation, unable to determine the measurement range in 3-D space. To overcome these limitations, we propose an imaging model-based calculating method. Specifically, we calculate the difference in 3-D coordinates corresponding to projector pixel pairs that have a  $2\pi$  phase shift in the projector phase but are imaged in the same camera pixel. Therefore the depth range in 3-D space can be quantitatively determined.

Different from existing studies, our proposed calculating method reveals that the measurement depth range is imbalanced, that is, the depth range in some regions is much narrower than the others. This phenomenon is referred to as the depth range imbalance (DRI) problem in this article. The DRI problem causes phase unwrapping errors and measurement failures in the narrow-depth-range regions, seriously affecting the application in real-world measurement scenarios. For the traditional constant-frequency fringes, though reducing the fringe frequency can increase the depth range, it sacrifices the overall accuracy. Obviously, there exist optimal fringe frequencies that satisfy the depth range requirements while maximizing the measurement accuracy. To determine the optimal frequencies, we propose to optimize the fringe frequency according to the system's geometric parameters. Unlike traditional constant frequency, the frequency of the optimized fringes varies throughout the encoding coordinates. Based on this, we propose the variable-frequency phase unwrapping (VFPU) method for high-speed 3-D shape measurement. The proposed VFPU method employs the variable-frequency fringes and geometric constraints to determine the absolute phase, requiring no additional patterns and achieving high measurement efficiency. Furthermore, the proposed method addresses the DRI problem and achieves higher accuracy. Our main contributions are summarized as follows.

- 1) We propose an imaging model-based method to calculate the measurement range of the geometric constraint-based phase unwrapping methods and reveal the DRI problem that causes measurement failure.

- 2) To address the DRI problem, we design a variable-frequency fringe pattern that adaptively determines the optimal frequencies through the system parameters and maximizes the measurement accuracy.
- 3) The proposed method requires no additional patterns and achieves high accuracy, high efficiency, and high robustness in complex shape measurement.

The remainder of this article is as follows. Section II discusses the principle. Section III discusses the simulation results. Section IV provides experimental results and discussion, and Section V concludes this work.

## II. PRINCIPLE

### A. Phase-Shifting Algorithm

The basic principle of phase-shifting algorithms is to actively project a sequence of sinusoidal fringe patterns and establish correspondence through phase information. Mathematically, the fringe pattern of an  $N$ -step phase-shifting algorithm with equal phase shift can be described as follows:

$$I_n^P(u^P, v^P) = I' + I'' \cos[\Phi(u^P, v^P) + 2\pi n/N] \quad (1)$$

where  $n = 0, 1, \dots, N-1$  and  $N$  is no less than 3.  $I_n^P(u^P, v^P)$  represents the intensity of projector pixel  $(u^P, v^P)$  in the  $n$ -th pattern.  $I'$  and  $I''$  denote the intensity bias and intensity modulation, respectively, and  $\Phi(u, v)$  is the initial encoding phase of pixel  $(u^P, v^P)$ . If fringes along the  $U^P$  axis are used,  $\Phi(u^P, v^P)$  can be expressed as

$$\Phi(u^P, v^P) = 2\pi u^P/T \quad (2)$$

where  $T$  is the fringe period (i.e., the number of pixels per fringe), and the fringe frequency is defined as  $f = 1/T$ . The fringe patterns are then projected and distorted by the measured surface, and the distorted phase in the captured images can be extracted by

$$\phi(u^c, v^c) = -\arctan \frac{\sum_{n=0}^{N-1} I_n^c(u^c, v^c) \sin(2\pi n/N)}{\sum_{n=0}^{N-1} I_n^c(u^c, v^c) \cos(2\pi n/N)} \quad (3)$$

where  $I_n^c(u^c, v^c)$  denotes the intensity of camera pixel  $(u^c, v^c)$  in the  $n$ th captured image. However, limited by the arctangent function, (3) only provides a wrapped phase ranging from  $-\pi$  to  $\pi$  with  $2\pi$  discontinuities, making it impossible to establish unique correspondence with the projector phase  $\Phi(u^P, v^P)$ . Therefore, the phase unwrapping algorithm is required to determine the absolute phase  $\Phi(u^c, v^c)$ . In essential, the phase unwrapping procedure determines the fringe orders and adds multiples of  $2\pi$  to the wrapped phase to eliminate phase ambiguity

$$\Phi(u^c, v^c) = \phi(u^c, v^c) + 2\pi k(u^c, v^c) \quad (4)$$

where  $k(u^c, v^c)$  denotes the fringe order for pixel  $(v^c, v^c)$ . The unwrapped phase is then used to recover the 3-D shape of the measured object through the imaging model, which will be introduced as follows.

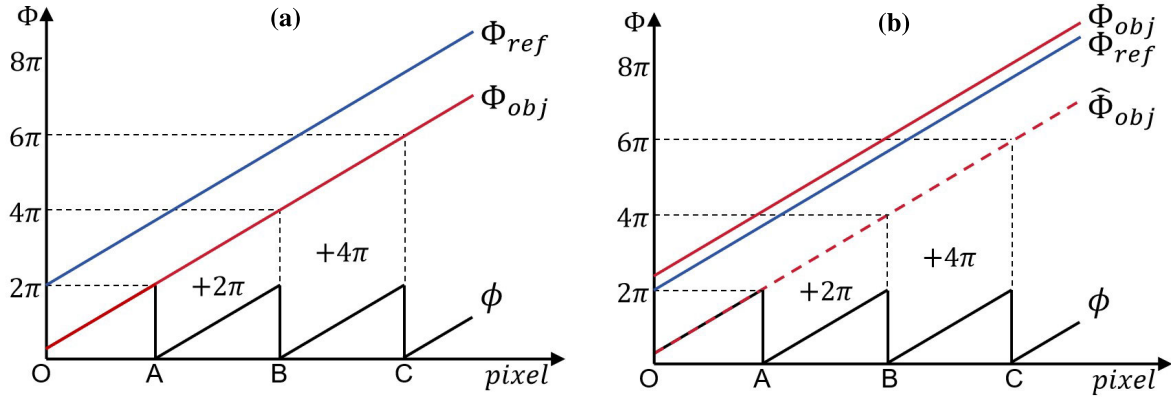


Fig. 1. Principle of phase unwrapping using the reference phase plane. (a) When the difference between the absolute phase  $\Phi_{obj}$  and the reference phase plane  $\Phi_{ref}$  does not exceed  $2\pi$ , the wrapped phase  $\phi$  can be unwrapped correctly. (b) Otherwise incorrect result  $\hat{\Phi}_{obj}$  with a  $2\pi$  phase gap would be introduced.

### B. Geometry Constraint-Based Phase Unwrapping

A typical DFP system consists of a camera and a projector, and the imaging lenses can be described using the well-known pin-hole model [36]. Mathematically, the measurement system can be described as

$$s^c \begin{bmatrix} u^c & v^c & 1 \end{bmatrix}^T = \mathbf{P}^c \begin{bmatrix} x^w & y^w & z^w & 1 \end{bmatrix}^T \quad (5)$$

$$s^p \begin{bmatrix} u^p & v^p & 1 \end{bmatrix}^T = \mathbf{P}^p \begin{bmatrix} x^w & y^w & z^w & 1 \end{bmatrix}^T \quad (6)$$

where  $s^c$  and  $s^p$  are two scale factors,  $(u^c, v^c)$  and  $(u^p, v^p)$  are the camera pixel and the corresponding projector pixel, respectively, and  $(x^w, y^w, z^w)$  denotes the 3-D world coordinates. The projection matrix  $P^c$  and  $P^p$  both have  $3 \times 4$  elements and can be determined through the DFP system calibration algorithm [37]. For each camera pixel  $(u^c, v^c)$ , (5) and (6) provide six equations with seven unknowns ( $s^c, s^p, u^p, v^p, x^w, y^w, z^w$ ); therefore, at least one additional constraint is required to recover the 3-D coordinates. In the DFP system, this problem is resolved by establishing the correspondence between the camera and projector pixels with the same absolute phase value [1].

To obtain the absolute phase  $\Phi(u^c, v^c)$ , the geometry constraint-based phase unwrapping (GCPU) method [26] generates a virtual reference plane with known phase and then determines the fringe order by calculating the phase difference. It is noteworthy that while An et al. [26] mainly discuss using the closest plane with the minimum phase as the reference, this article considers the furthest plane with the maximum phase to match our real-world measurement condition, where the measured objects are placed upon the reference plane, between the reference plane and the camera. Though different symbols are used, the concepts behind them are identical. Similar conditions also have been discussed in [35] and [38].

In general, the pre-defined reference plane is perpendicular to the optical axis of the camera and denoted as  $z^w = z_{ref}$ . Substituting  $z_{ref}$  into (5) and (6), all the other unknowns ( $s^c, s^p, u^p, v^p, x^w, y^w$ ) can be uniquely determined. Once  $(u^p, v^p)$  is obtained, the absolute reference phase  $\Phi_{ref}(u^c, v^c)$  corresponding to  $z_{ref}$  can be calculated using (2). Apparently, the reference phase is a function of  $z_{ref}$ , the fringe period  $T$ ,

and the projection matrices, that is,

$$\Phi_{ref}(u^c, v^c) = f(z_{ref}, T, P^c, P^p). \quad (7)$$

The principle of phase unwrapping using the reference phase plane is illustrated in Fig. 1(a). The blue solid line represents the reference phase plane  $\Phi_{ref}$ , while the black solid line represents the wrapped phase  $\phi$ . For pixels between O and A,  $\Phi_{ref} - \phi < 2\pi$ , no operation is required; between A and B,  $2\pi < \Phi_{ref} - \phi < 4\pi$ , then  $2\pi$  needs to be added; between point B and C,  $4\pi < \Phi_{ref} - \phi < 6\pi$ , then  $4\pi$  needs to be added. Similar operations are applied to the rest; therefore, the full-field  $2\pi$  discontinuities can be eliminated, and the absolute phase  $\Phi_{obj}$  can be obtained as the red solid line in Fig. 1(a). The calculation process can be expressed as

$$k(u^c, v^c) = \left\lfloor \frac{\Phi_{ref}(u^c, v^c) - \phi(u^c, v^c)}{2\pi} \right\rfloor \quad (8)$$

where  $\lfloor \cdot \rfloor$  represents the floor operation, which returns the largest integer less than or equal to the input. As the fringe order is obtained, the unwrapped phase can be determined by (4).

The GCPU method requires no additional patterns or complex computation, achieving higher efficiency than traditional approaches. However, it suffers from a measurement range limitation problem: the object phase plane  $\Phi_{obj}$  should be within  $[\Phi_{ref} - 2\pi, \Phi_{ref}]$ . As a failure case, Fig. 1(b) shows that, when the object phase exceeds  $\Phi_{ref}$ , the unwrapped result  $\hat{\Phi}_{obj}$  would be  $2\pi$  less than the true phase, leading to incorrect measurement results. The above analysis illustrates the measurement range in terms of phase, while Fig. 2(a) illustrates how to determine the corresponding range in terms of depth. The black solid line and black dashed line represent the reference and the upper-bound object planes, respectively, and the adjacent red serrated line represents the phase distribution. The blue solid line and blue dashed line represent the projection light and the captured light, respectively, between which the angle is  $\theta$ , and the spatial span of one projected fringe period is  $T_s$ . Point A on the object phase plane and point C on the reference plane are imaged by the same camera pixel, but have  $2\pi$  phase shift. Through simple trigonometrical

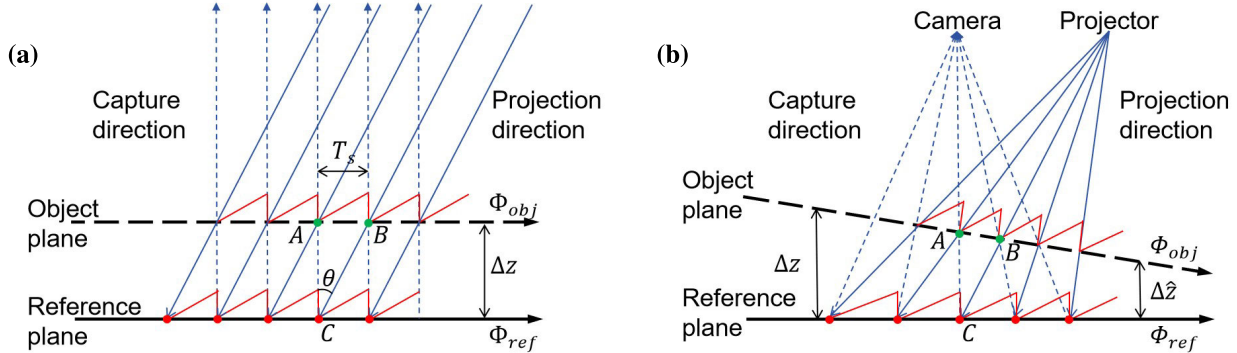


Fig. 2. Measurement depth range model. (a) Existing studies take the capture light and projection light as parallel, and the depth range is constant throughout. (b) According to the pin-hole lens model, the angle and the fringe spans vary along the coordinates; therefore, the depth range is imbalanced.

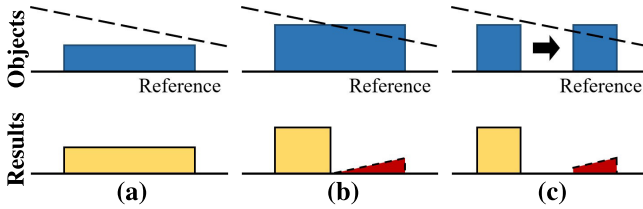


Fig. 3. Measurement results of different objects. (a) Correct measurement. (b) Incorrect measurement. (c) Correct measurement on the left side, but incorrect when moved to the right.

derivations, the measurement depth range can be obtained as

$$\Delta z = T_s / \tan \theta. \quad (9)$$

Increasing the fringe period would enlarge  $T_s$  and thus extend the measurement depth range. However, this also degrades phase quality and increases measurement error, which is undesirable for high-accuracy measurements [27].

### C. Variable-Frequency Phase Unwrapping

Existing methods often assume that light rays are parallel; however, this assumption is not valid for typical DFP systems equipped with pin-hole lenses. As illustrated in Fig. 2(b), since light rays diverge from the optical centers of the camera and projector, the angle between the capture and projection lights varies, and the fringe spans on the object plane would also be changed. Consequently, the object plane is not parallel to the reference plane, resulting in an imbalanced depth range. In the case of Fig. 2(b), the depth range on the right side is narrower than that on the left side.

The DRI problem causes abnormal measurement failures. Fig. 3 illustrates measurement results of objects with different sizes. In Fig. 3(a), when the block lies entirely beneath the object plane, the shape is recovered successfully. However, in Fig. 3(b), despite the block's height being less than the maximum depth, the right half is measured incorrectly due to phase unwrapping failure. Furthermore, in Fig. 3(c), the small block is successfully measured when placed on the left side, but unsuccessfully on the right, indicating that the measured object must be carefully placed. Moreover, the issue of DRI complicates the measurement process, as the measurement depth range cannot be quantitatively estimated. These

drawbacks limit its application in practical 3-D measurement specifically in automated scenarios.

To quantitatively evaluate the imbalanced depth range, we develop an imaging model-based calculating method. We adopt the DFP imaging model to determine the upper-bound object plane, which also satisfies (5) and (6). For each point on the object plane, there exists a corresponding point on the reference plane, and both are imaged onto the same pixel by the camera, but with a  $2\pi$  shift in the absolute phase as defined by the projector. As illustrated in Fig. 2(b), the phase of point C on the reference plane is equal to that of point B on the object plane, and is  $2\pi$  greater than point A corresponding to the same camera pixel. This relationship can be mathematically expressed as

$$\Phi_{obj}(u^c, v^c) = \Phi_{ref}(u^c, v^c) - 2\pi. \quad (10)$$

If fringes along the  $U^P$  direction are used, the projector pixel corresponding to the object plane can be determined by

$$u_{obj}^P = u_{ref}^P - T \quad (11)$$

where  $u_{ref}^P$  is the projector pixel corresponding to the reference plane, which is obtained in solving (7), and  $T$  is the fringe period.

Apparently,  $u^P = u_{obj}^P$  provides an additional constraint for solving (5) and (6); therefore, all the unknowns can be uniquely determined. Using  $z^w = z_{obj}(u^c, v^c)$  to denote the object plane, we obtain the measurement depth range by

$$\Delta z(u^c, v^c) = |z_{obj}(u^c, v^c) - z_{ref}| \quad (12)$$

where  $|\cdot|$  represents the absolute value function.

Fig. 4 illustrates a 3-D view of the imbalanced measurement depth range calculated from (12), where the blue and yellow planes are the reference plane and the non-parallel object plane, respectively. From Fig. 4, objects that can be accurately measured in areas with a large depth range may exceed the boundaries in areas with a smaller depth range, leading to measurement failures. To ensure measurement performance across the entire field of view, the measurement depth range should be uniformly distributed. In other words, the upper-bound object plane should be parallel to the reference plane, as shown by the green plane in Fig. 4.

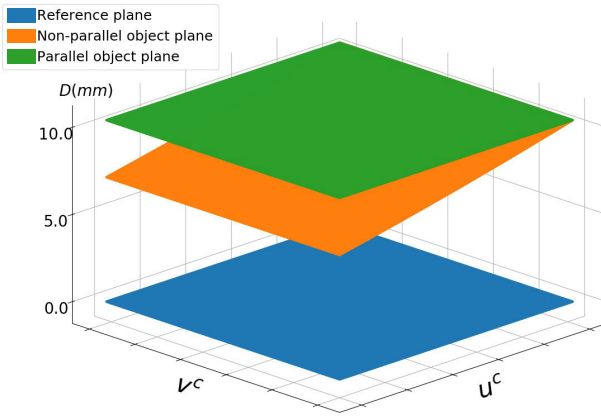


Fig. 4. Quantitatively calculated depth range distribution.

As (10) and (11) indicate, for each camera pixel, the measurement depth range is the depth difference between the spatial coordinates corresponding to two corresponding projector pixels. For the conventional constant-frequency method, these two projector pixels have a phase bias of  $2\pi$  and a pixel bias equal to the fringe period  $T$ . Therefore, increasing the fringe period, that is, decreasing the fringe frequency, can expand the depth range. However, a lower fringe frequency leads to degradation in measurement accuracy [14]. Considering the imbalanced depth range, there exist optimal fringe frequencies for each pixel that ensures a consistent depth range while simultaneously maximizing measurement accuracy. To determine the optimal frequencies, we first calculate the projector pixel corresponding to a virtual object plane that is parallel to the reference plane. According to the previous analysis, for the object plane at  $z_w = z_{\text{obj}}$ , the projector pixels can be uniquely determined by solving (5) and (6). Therefore the variable pixel bias, denoted as  $T(u^p, v^p)$ , is a function of  $z_{\text{ref}}$ ,  $z_{\text{obj}}$ , and the projection matrices, that is,

$$T(u^p, v^p) = f(z_{\text{ref}}, z_{\text{obj}}, P^c, P^p). \quad (13)$$

It is noteworthy that  $z_{\text{ref}}$  and  $z_{\text{obj}}$  are both given artificially according to the measurement requirements. Therefore, the measurement depth range is constant and can be determined by

$$\Delta z_c = z_{\text{ref}} - z_{\text{obj}}. \quad (14)$$

Given  $z_{\text{obj}}$ , the corresponding  $x^w$  and  $y^w$  for each camera pixel  $(u^c, v^c)$  can be determined by solving (5), which is expressed as

$$\begin{bmatrix} x^w \\ y^w \end{bmatrix} = \mathbf{M}^{-1} b \quad (15)$$

where

$$\mathbf{M} = \begin{bmatrix} p_{31}^c u^c - p_{11}^c & p_{32}^c u^c - p_{12}^c \\ p_{31}^c v^c - p_{21}^c & p_{32}^c v^c - p_{22}^c \end{bmatrix}$$

$$b = \begin{bmatrix} p_{14}^c - p_{34}^c u^c - (p_{33}^c u^c - p_{13}^c) z_{\text{obj}} \\ p_{24}^c - p_{34}^c v^c - (p_{33}^c v^c - p_{23}^c) z_{\text{obj}} \end{bmatrix}. \quad (16)$$

Here  $p_{ij}^c$  denotes the matrix parameters of  $\mathbf{P}^c$  in  $i$ th row and  $j$ th column. By substituting  $(x^w, y^w, z^w)$  into (6), the

corresponding projector pixel along the  $U^p$  axis can be determined by

$$u_{\text{obj}}^p = \frac{p_{11}^p(x)^w + p_{12}^p y^w + p_{13}^p z^w + p_{14}^p}{p_{31}^p x^w + p_{32}^p y^w + p_{33}^p z^w + p_{34}^p}. \quad (17)$$

Then, we obtain the projector pixel bias in the  $U^p$  axis as

$$T(u^p, v^p) = u_{\text{ref}}^p - u_{\text{obj}}^p. \quad (18)$$

Notably, the phase difference between  $u_{\text{ref}}^p$  and  $u_{\text{obj}}^p$  is  $2\pi$ , which can be mathematically expressed as

$$\Phi(u_{\text{ref}}^p) - \Phi(u_{\text{obj}}^p) = 2\pi. \quad (19)$$

Since the fringe frequency can be expressed as the derivative of the fringe phase divided by  $2\pi$ , the fringe phase can be determined by finding the integral of the fringe frequency multiplied by  $2\pi$ . Assuming that the phase value at the pixel origin is zero, the fringe phase along the  $U^p$  axis satisfies

$$\Phi(u^p) = 2\pi \int_0^{u^p} f(u) du \quad (20)$$

where  $f(u)$  denotes the fringe frequency at pixel  $u$ . Then, (19) can be converted to

$$2\pi \int_{u_{\text{obj}}^p}^{u_{\text{ref}}^p} f(u^p) du^p = \Phi(u^p) \Big|_{u_{\text{obj}}^p}^{u_{\text{ref}}^p} = 2\pi. \quad (21)$$

Considering its monotonicity and continuity, we use polynomials to represent  $\Phi(u^p)$ . Since each  $u_{\text{ref}}^p - u_{\text{obj}}^p$  sample satisfies (21), the polynomial parameters can be estimated through the popular least-square algorithm. It is noteworthy that the obtained  $\Phi(u^p)$  is relative phase for pixels in between  $[u_{\min}^p, u_{\max}^p]$ , where  $[u_{\min}^p, u_{\max}^p]$  are the minimum and maximum of all  $u_{\text{ref}}^p - u_{\text{obj}}^p$  samples, respectively. Therefore, we first calculate the derivative of  $\Phi(u^p)$  to determine the fringe frequency in between  $[u_{\min}^p, u_{\max}^p]$ , and set constant-frequency value for the rest of the pixels. Specifically, the entire frequency along the  $U^p$  direction is as follows:

$$f(u^p) = \begin{cases} f(u_{\min}^p), & u^p < u_{\min}^p \\ \frac{d\Phi(u^p)}{du^p}, & u_{\min}^p \leq u^p \leq u_{\max}^p \\ f(u_{\max}^p), & u^p > u_{\max}^p. \end{cases} \quad (22)$$

After obtaining the fringe frequency, the encoding phase can be determined using (20). Since the phase does not increase linearly with the coordinates, a look-up table (LUT) is established to store the phase values to simplify calculations in the decoding procedure. Next, the encoding fringe patterns can be determined through (1).

The proposed VFPU method is friendly to existing DFP systems since the conventional phase analysis methods can still be used in the decoding process. Firstly, the wrapped phase is determined from (3), and the reference phase plane is generated for phase unwrapping. The major difference lies in the pixel-matching procedure: the corresponding projector coordinates are determined by referring to the pre-established phase LUT, and then the 3-D shape is recovered.

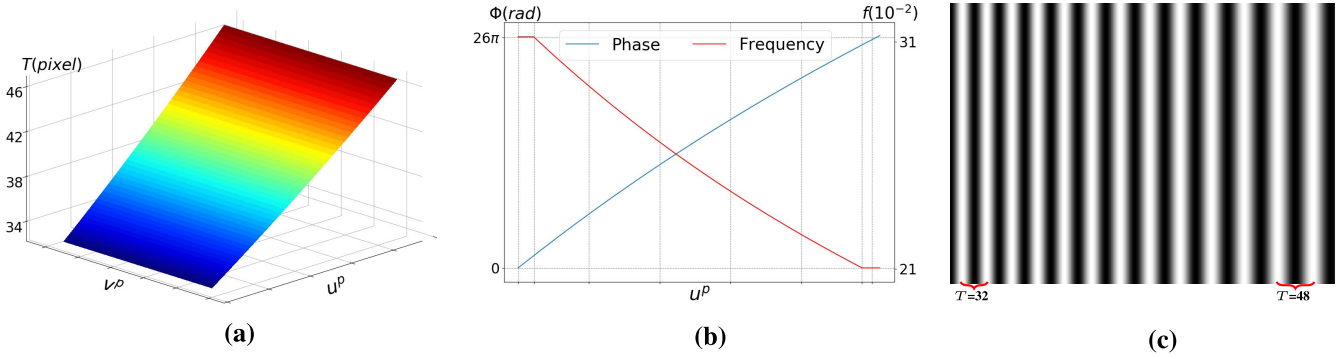


Fig. 5. Simulation results. (a) Variable projector pixel bias. (b) Fringe frequency and the corresponding phase distribution in the  $U^p$  axis. (c) Variable-frequency fringe pattern.

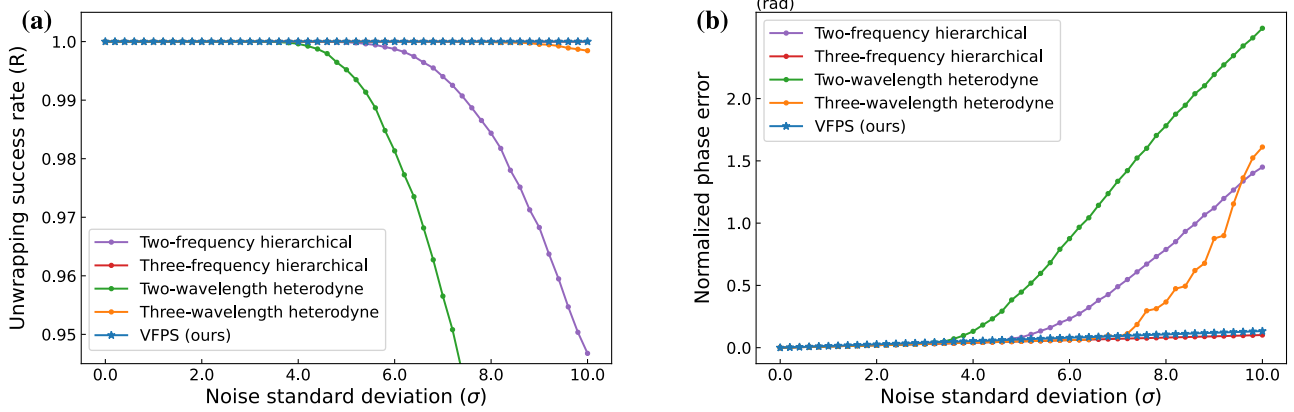


Fig. 6. Simulation results in the presence of noise. (a) Phase unwrapping success ratio. (b) Phase error.

### III. SIMULATIONS

We conduct simulations to validate the feasibility and robustness of the proposed method. Our simulated measurement system comprises a camera and projector, both with resolutions of  $512 \times 512$  and focal lengths of 20 mm. The devices are positioned at an angle of  $\pi/6$  to each other, with a reference plane established at 180 mm perpendicular to the camera. The projection matrices for the camera and projector are calculated using the pin-hole model [36].

According to the principle of depth range calculation, for constant-frequency sinusoidal patterns with a period of 32 pixels, the maximum and minimum depth ranges are 10.3 and 7.2 mm, respectively. Therefore, we set the upper-bound object plane at 10.3 mm. Fig. 5(a) illustrates how pixel bias in (18) varies with projector coordinates. Fig. 5(b) depicts the fringe frequency (in red) and the encoding phase (in blue), showing the variation of fringe frequency with pixel coordinates. Finally, Fig. 5(c) displays one of the VFPU patterns, which demonstrates variations in the fringe spans along the  $U^p$  axis, ranging from 32 pixels on the left to 48 pixels on the right.

We assess performance under noisy conditions by comparing the proposed VFPU method with widely used temporal unwrapping techniques [14], including two- and three-frequency hierarchical methods (labeled MF-2 and MF-3, respectively), and two- and three-wavelength heterodyne methods (labeled MW-2 and MW-3, respectively). We generate a plane 175 mm perpendicular to the camera as the

measurement object. The ground-truth phase is determined using simulated calibration parameters, and the captured fringe patterns are set with an average intensity of 128 and fringe modulation of 70, consistent with [14]. We add Gaussian-distributed random noise to these patterns and compare the phase error and unwrapping success rates. The results in Fig. 6(a) indicate that the phase unwrapping success rate for the MW-2, MW-3, and MF-2 methods declines as noise levels increase. In contrast, the MF-3 and VFPU methods maintain robust performance. Notably, the MF-3 method utilizes 12 patterns, while the VFPU method requires only 4 patterns. As depicted in Fig. 6(b), although the MF-3 method slightly outperforms the VFPU method in terms of phase error, the VFPU method is significantly more efficient, using only one-third the number of patterns. The results demonstrate the robustness and efficiency of the proposed VFPU method.

### IV. EXPERIMENTS AND DISCUSSION

#### A. Experiment Setup

To experimentally evaluate the proposed VFPU method, we develop a DFP system consisting of a digital light processing projector (Texas Instruments DLP LightCrafter 4500, 405 nm wavelength light) and a CMOS camera (FLIR BFLY-PGE-50S5M-C). The resolutions of the projector and camera are  $912 \times 1140$  and  $2448 \times 2048$ , respectively, and the focal lengths are 28 and 25 mm, respectively. This DFP system is developed for microscopic objects and the field of view is

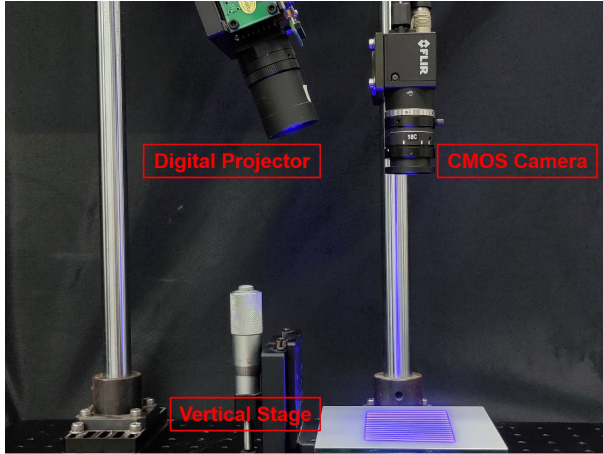


Fig. 7. Photograph of the DFP measurement system.

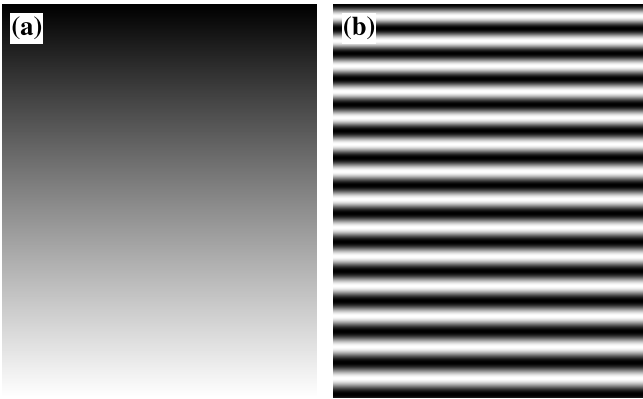


Fig. 8. Variable-frequency pattern design in the experiments. (a) Variable-frequency phase distribution. (b) One of the variable-frequency fringe patterns.

approximately  $40 \times 50$  mm. The photograph of the system is shown in Fig. 7. To acquire the projection matrices for the camera and projector, the method proposed in [37] is adopted for calibration.

The virtual reference plane is set to 175 mm perpendicular to the camera. For the standard sinusoidal fringe with 16 periods, the maximum depth range the geometric constraints can handle is 9.0 mm according to (12). Therefore, we select 9.0 mm as the depth range to design the variable-frequency fringes. The encoding phase is illustrated in Fig. 8(a) and is stored in an LUT with 50 sample elements per pixel for pixel matching. Fig. 8(b) shows one of the variable-frequency fringe patterns. Unless otherwise specified, we employ four-step phase shifting for all the methods in the following experiments. The 32-step three-frequency hierarchical method is implemented to obtain the ground-truth absolute phase.

#### B. Comparison With Traditional Methods

To evaluate the measurement precision of the system, we select a standard plane as the measurement object. We obtain the absolute phase through the proposed VFPU method and calculate the 3-D point clouds of the standard plane. We use the point clouds to fit an ideal plane and calculate the residual error. Fig. 9 shows the full-field error

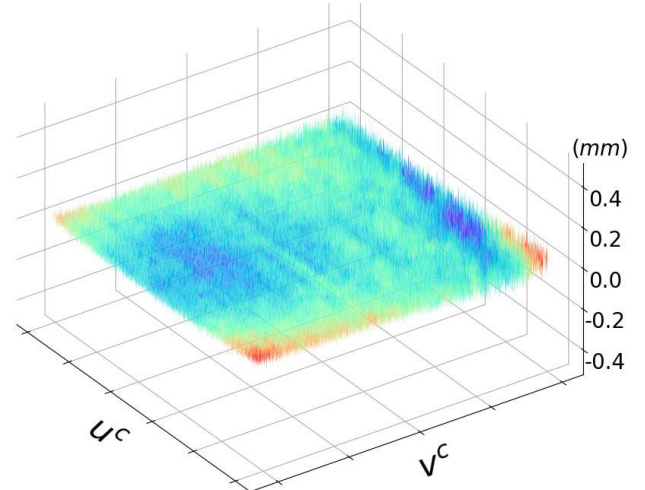


Fig. 9. Measurement error distribution on the standard plane.

TABLE I  
PIXEL-MATCHING ACCURACY USING LUT

Method	Number of patterns	LUT elements per pixel	RMSE (pixel)
4-step VFPS	4	10	0.0959
4-step VFPS	4	20	0.0928
4-step VFPS	4	50	0.0921
4-step VFPS	4	100	0.0921
4-step MF-3	12	-	0.0871

distribution, and the root mean square error (RMSE) is 0.0177 mm. We then experimentally evaluate the impact of the number of LUT elements on measurement accuracy. We find the pixel coordinates corresponding to the unwrapped phase from the LUT and then calculate the pixel-matching error relative to the ground truth. As shown in Table I, the pixel-matching error decreases as the number of LUT elements per pixel increases, stabilizing when it exceeds 50 elements per pixel. For comparative analysis, we also calculated the matching error using the MF-3 method, which performs better than the VFPU method by 0.005 pixels. This difference can be attributed to the VFPU method's frequency modification to address the imbalanced depth ranges. However, it is noteworthy that the VFPU method requires only one-third the number of patterns compared to the MF-3 method.

We then compare the proposed VFPU method with widely used phase unwrapping methods through plane measurement experiments. In addition to the sinusoidal fringe-based methods, we explore several discrete fringe-based methods, including the phase-encoding (PC) method [39], the Gray-code (Gray) method [15], the misaligned Gray-code (MGC) method [40], and the generalized Tri-PU method [41]. To evaluate the measurement performance under noisy conditions, we add Gaussian-distributed noise with different standard deviations to the captured fringe patterns and calculate the phase error and unwrapping success rate. The experimental results in Fig. 10

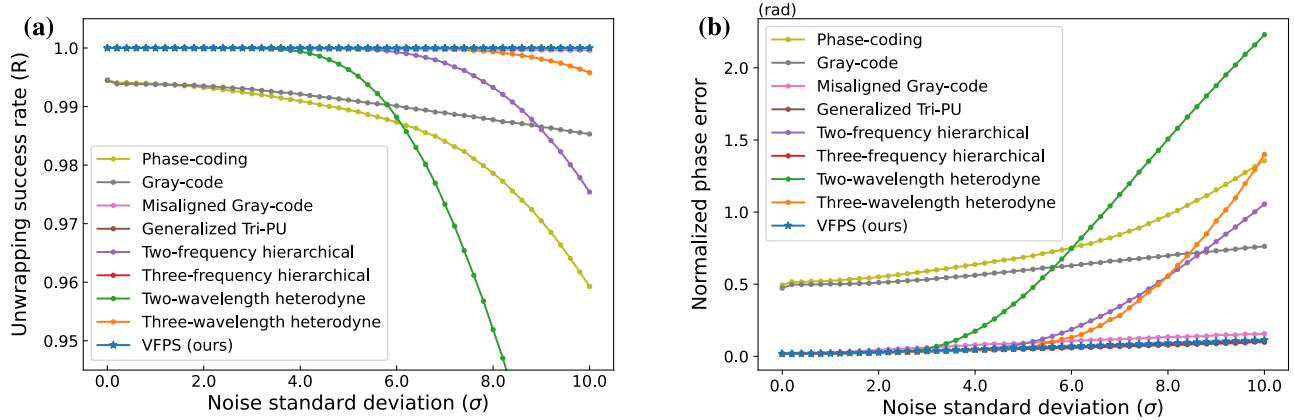


Fig. 10. Experimental results in the presence of noise. (a) Phase unwrapping success ratio. (b) Phase error.

are consistent with the simulations. Among phase unwrapping methods based on sinusoidal fringes, the MF-3 method is more stable than others, while the heterodyne methods are observed to be more sensitive to noise due to higher noise amplification [14]. In methods based on discrete fringes, the phase-coding and Gray-code methods are affected by jump errors, leading to a decrease in the unwrapping success rate as noise increases. To address the mismatching problem, the misaligned Gray-code method pre-shifts the Gray-code fringes by half a period before projection, and the generalized Tri-PU method divides each period of fringe order into three parts, performing phase unwrapping individually. These adaptations effectively address the jump errors problem. Regarding the proposed VFPU method, the unwrapping success rate remains stable, even with the fewest patterns due to its immunity to additional noise from extra patterns and noise amplification caused by phase weighting.

We then evaluate the computational efficiency of various methods through plane measurement experiments conducted on a laptop with an Intel Core i7-10750H CPU. Each method is executed a thousand times to determine average computational times and standard deviations accurately, and the results are detailed in Fig. 11. The computational time for the proposed VFPU method is 0.1528 s, which is faster than the other methods. Furthermore, our method achieves lower memory usage, requiring only 47.9 MB. These results demonstrate the superior computational efficiency and memory consumption of our method. The reason can be attributed to two factors: first, the VFPU method requires only four images, whereas others need at least eight; second, it directly calculates the fringe order, avoiding intermediate computation such as the low-frequency phase in multifrequency hierarchical methods and the tripartite phase maps in the Tri-PU method. These advantages make our method highly effective for practical 3-D measurement, offering enhanced measurement speed and reduced system load.

In the second experiment, a printed circuit board (PCB) is selected as the measured object. As the photograph shown in Fig. 12(a) suggests, measuring the PCB is very challenging for DFP systems due to the high dynamic range, drastic height change, and severe inter-reflection. Fig. 12(b) shows

one of the captured fringe patterns, and Fig. 12(c) shows the wrapped phase calculated from these patterns. The fringe order is estimated pixel-by-pixel and shown in Fig. 12(d). By combining the wrapped phase and the fringe order, the absolute phase and the depth map are reconstructed, and the results are illustrated in Fig. 12(e) and (f), respectively. As can be seen, the proposed method recovers the geometry of the PCB despite the aforementioned challenges.

Furthermore, several widely used methods are adopted to measure the same PCB for comparison. All these methods use sinusoidal patterns with 16 periods to obtain the wrapped phase, but determine the fringe order using different extra patterns such as sinusoidal fringes, stair-phase fringes, or Gray-code fringes. For the multifrequency method and the phase-coding method, the shifting steps are both set to 4. For the Gray-code method and the generalized Tri-PU method, four extra binary patterns are required to encode the 16 fringe orders. Fig. 13 shows the measurement results using different methods, and the top-right rectangles are the enlarged views. We first adopt the two-frequency hierarchical method, and the result illustrated in Fig. 13(a) shows some artifacts, which are primarily caused by the random noise amplified by the phase weighting. To address these artifacts, we employ more patterns to conduct the three-frequency hierarchical method. The results in Fig. 13(b) suggest that the errors are effectively reduced. We also conduct the two- and three-wavelength heterodyne methods; the results in Fig. 13(c) and (d) suggest that the hierarchical method outperforms the heterodyne method, aligning well with existing studies [14]. However, though more patterns are used, the unwrapping errors cannot be completely resolved due to the phase weighting procedure. Fig. 13(b) and (c) shows the measurement results of the phase-encoding method and the Gray-code method, respectively. Both methods suffer from strip-like depth artifacts (also known as jump errors) because the fringe order and the wrapped phase are not perfectly matched, which is caused by optical defocus, motion blur, and surface texture [42]. The results in Fig. 13(g) and (h) show that, compared with the original Gray-code method, most jump errors are effectively reduced. However, the noisy wrapped phase may induce new unwrapping errors in the height-disconnected regions.

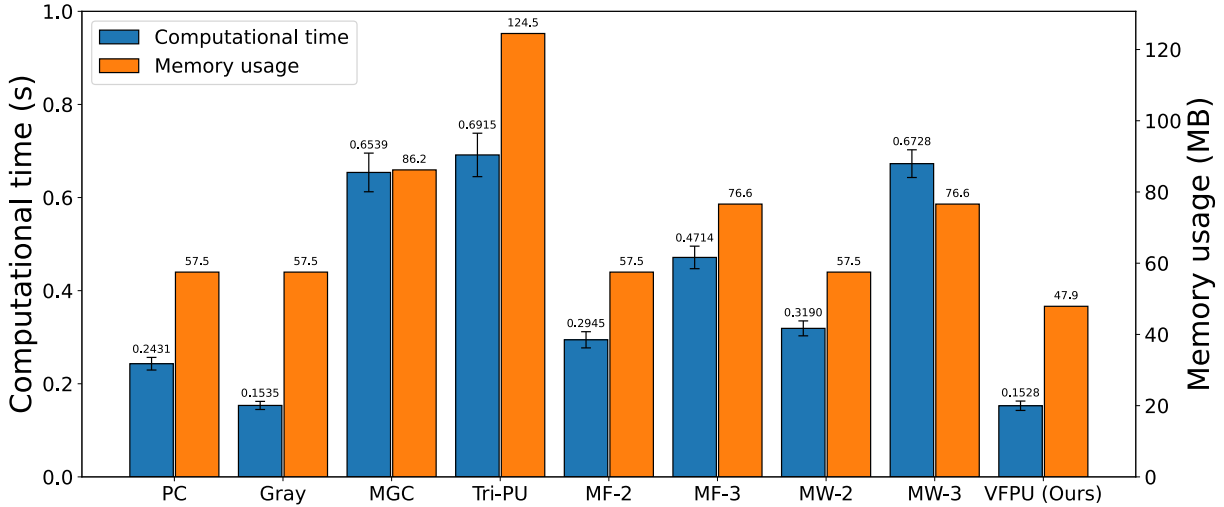


Fig. 11. Measurement efficiency comparison.

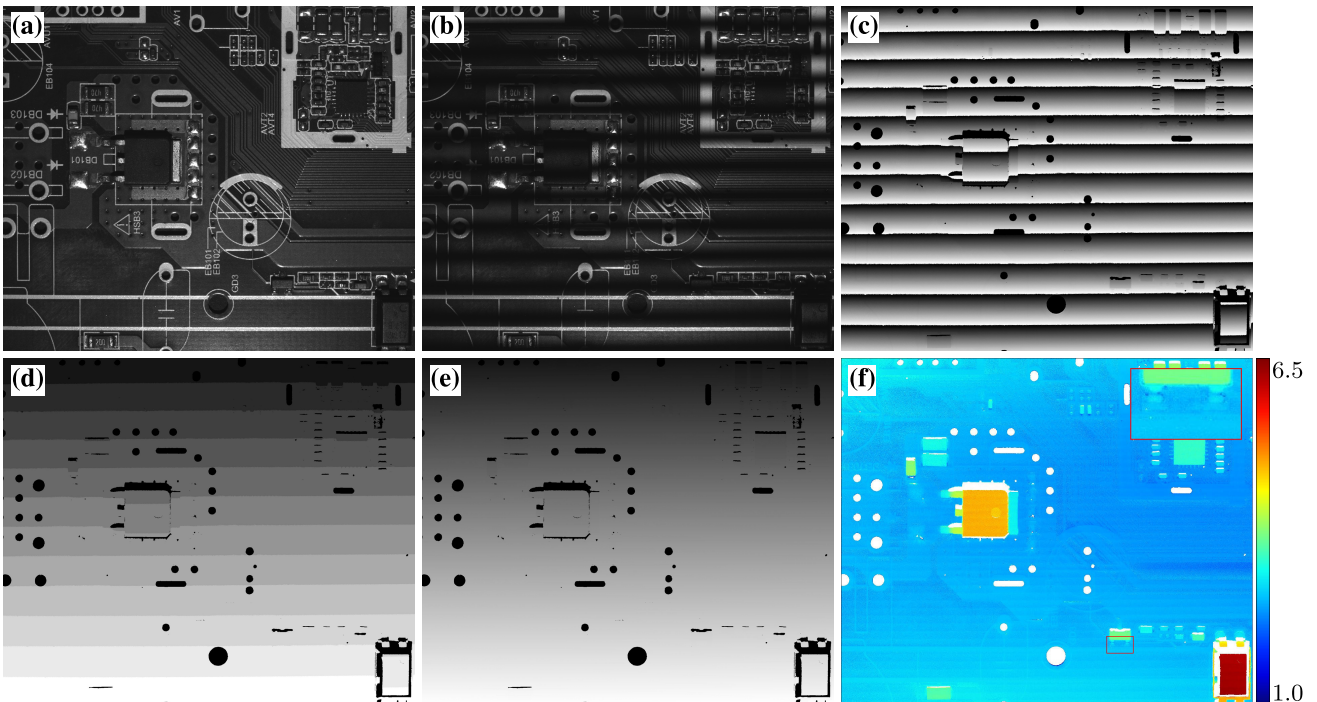


Fig. 12. Measurement results of the PCB. (a) Photograph. (b) One of the captured fringe patterns. (c) Wrapped phase. (d) Fringe order. (e) Unwrapped phase. (f) Recovered depth. The top-right red rectangle shows the enlarged view.

To make a quantitative comparison of these methods, we calculate the root mean square error according to the ground-truth phase map. The results, presented in Table II, demonstrate that the proposed VFPU method achieves both higher measurement speed and accuracy than traditional methods. Specifically, while the traditional methods require 8 or 12 fringe patterns to obtain the absolute phase, the proposed method only needs 4, achieving at least twice the measurement speed of the traditional methods. Moreover, the proposed method exhibits fewer phase errors than other methods. Specifically, the number of unwrapping-error pixels for the proposed VFPU method is 2, significantly fewer than those observed in traditional methods, and the corresponding RMSE is also

lower ( $0.0657$  rad), suggesting its advantages in measurement accuracy and efficiency. We further increase the shifting step to eight to compare the accuracy with equal patterns, and the RMSE further decreases to  $0.0531$  rad. Compared to experiments conducted on the white plane, our proposed VFPU method significantly outperforms the MF-3 method in measuring PCBs, demonstrating its higher robustness when dealing with objects that have complex geometries and high dynamic ranges.

### C. Comparison With the Conventional GCPU Method

We compare the proposed VFPU method with the conventional GCPU methods to verify the advantages of the

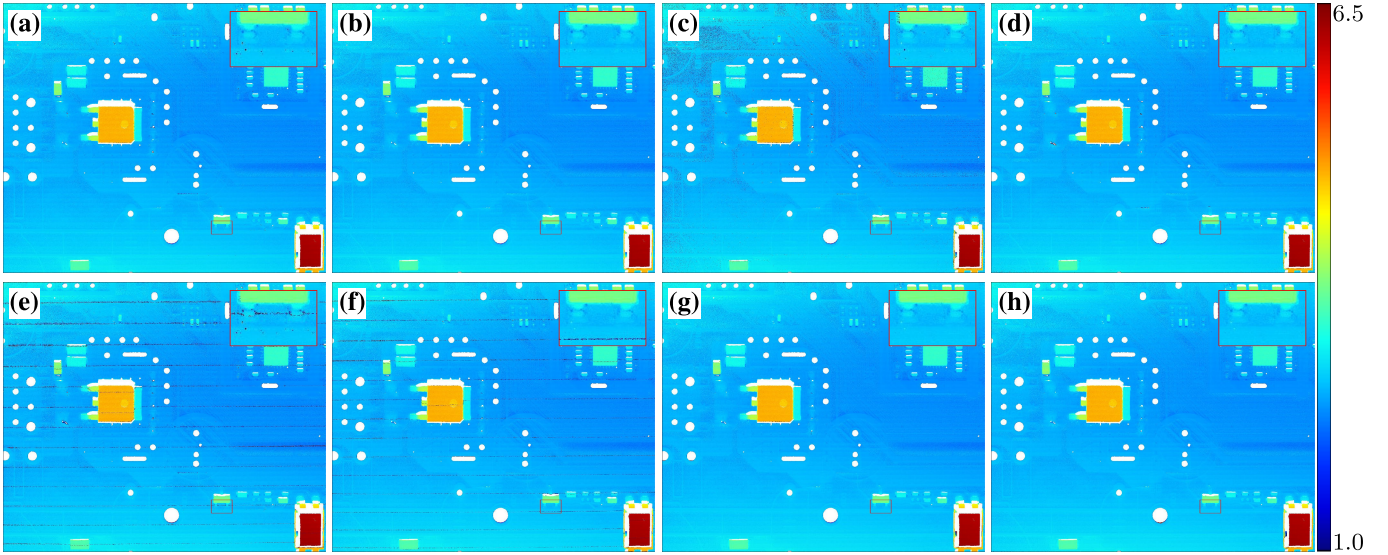


Fig. 13. Measurement results using the traditional methods. (a) Two-frequency hierarchical method. (b) Three-frequency hierarchical method. (c) Two-frequency heterodyne method. (d) Three-frequency heterodyne method. (e) Phase-coding method. (f) Gray-code method. (g) Misaligned Gray-code method. (h) Generalized Tri-PU method. The top-right red rectangles show the enlarged view.

TABLE II  
MEASUREMENT OF THE PCB

Method	Number of patterns	Number of error unwrapping	RMSE (rad)
4-step MF-2	8	2791	0.1640
4-step MF-3	12	20	0.0721
4-step MW-2	8	57170	0.7004
4-step MW-3	12	1913	0.3967
PC	8	53871	0.6548
Gray	8	35862	0.5042
MGC	8	876	0.1003
Tri-PU	8	1040	0.1135
<b>4-step VFPU</b>	<b>4</b>	<b>2</b>	<b>0.0657</b>
<b>8-step VFPU</b>	<b>8</b>	<b>0</b>	<b>0.0531</b>

variable-frequency fringes. In the first experiment, we utilized two methods to measure a step-shaped object with a significant height disparity. Fig. 14 presents the experimental results, where Fig. 14(a) and (b), respectively, displays the fringe patterns captured using the traditional GCPU method and the proposed VFPU method, illustrating the occlusion of the steps causing discontinuities in the fringes. Fig. 14(c) and (d) shows the corresponding reconstructed results for the two methods. The traditional GCPU method fails to accurately reconstruct the step due to the DRI that leads to phase unwrapping errors. In contrast, the proposed VFPU method successfully reconstructs the object, demonstrating that the VFPU method is capable of effectively handling objects with height variations and discontinuities.

In the second experiment, we place a white plane on a height-adjustable vertical stage, starting at an initial height of 4 mm above the reference plane and increasing it by 1.5 mm each time. Fig. 15 shows the measurement results. The existing GCPU method recovers the plane correctly when it is relatively

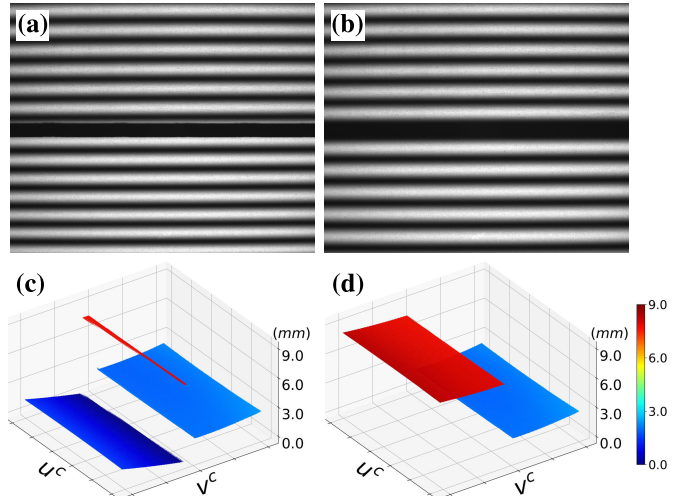


Fig. 14. Measurement results for a step-shaped object. (a) and (b) Captured fringe pattern for the GCPU method and the VFPU method, respectively. (c) and (d) Reconstructed depth by the GCPU method and the VFPU method, respectively.

low (e.g., 4 and 5.5 mm); however, the measurement fails as the platform increases to 7 mm and beyond. Specifically, the incorrectly measured parts sharply go down to almost 0, that is, the reference plane, which is consistent with Fig. 3(b). On the contrary, our proposed method correctly recovers the depth at different heights. Moreover, we compare the measurement error for these two methods at the initial height, where the RMSE is 0.1000 rad for the GCPU method and 0.0964 rad for the proposed VFPU method. These results demonstrate the DRI problem for the traditional GCPU method, as well as our superiority in both the measurement range and accuracy.

To compare the measurement performance in a real-world industrial scenario, we select a PCB with a high-definition multimedia interface (HDMI), which is relatively high, as the tested object. As shown in the upper row of Fig. 16, when

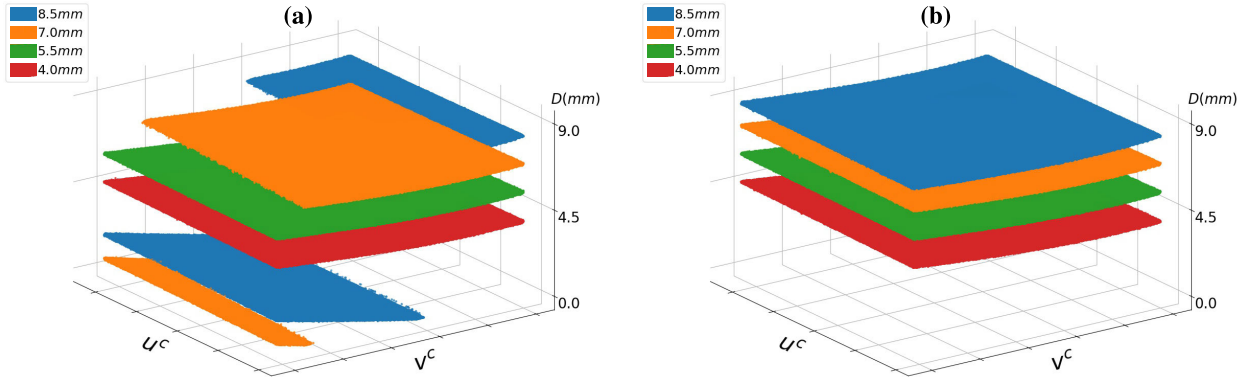


Fig. 15. Measurement results for planes at different heights of (a) conventional GCPU method and (b) our proposed method.

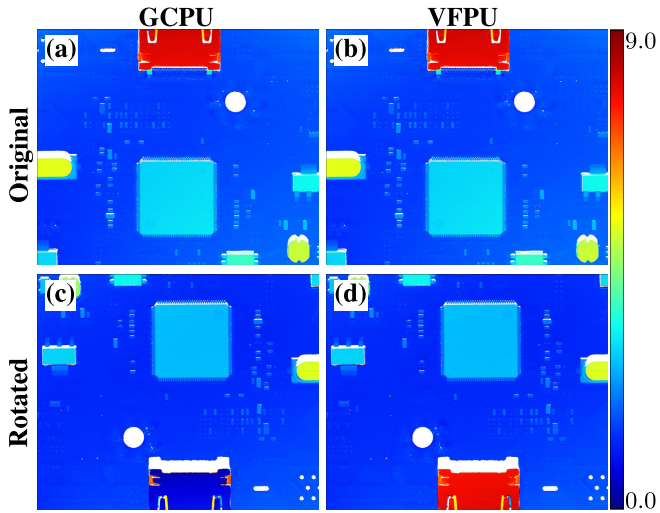


Fig. 16. Measurement result on the PCB with a tall HDMI. (a) and (b) Results at the original position. (c) and (d) Results after rotating the PCB for  $180^\circ$  and keeping the height unchanged.

the interface is at the top, both methods correctly recover the 3-D shape; however, when the PCB is rotated by  $180^\circ$  while maintaining the height unchanged, as shown in the lower row, the proposed VFPYU method is not affected, but the traditional GCPU method fails to measure the HDMI correctly. This is because, for the traditional GCPU method, the measurement range at the bottom is smaller than the HDMI's height, resulting in incorrect phase unwrapping, which is consistent with Fig. 3(c). These results suggest that the DRI problem dramatically affects practical applications since correct measurement results can only be obtained by manually placing tall objects at specific positions. However, the measurement systems are expected to handle flexible measurement objects and automatically complete 3-D measurements with as little manual intervention as possible. Obviously, it is challenging for the GCPU method to handle automated measurement scenarios such as production lines, while our proposed method achieves robust and efficient measurement.

#### D. Discussion

In addition to the superiorities in accuracy, robustness, and measurement depth range, the proposed VFPYU method presents an important advantage in that the measurement depth

range is throughout identical, and can be adjusted precisely, which is very important in practical measurement. For the traditional constant-frequency fringes, since the effective range varies in the entire measurement field, it is very inconvenient to determine the actual measurement range at specific positions to judge whether the measurement is applicable. While increasing the fringe period enhances the depth range at the narrower side to satisfy the depth requirements, the overall accuracy decreases. On the contrary, our proposed method calculates the optimal variable frequencies based on the system geometry parameters and measurement range requirements, not only avoiding the waste of measurement range (i.e., the over-broad side in the imbalanced depth range) but also making the fringes as densest as possible to achieve higher accuracy.

The DRI problem arises due to the non-parallel light characteristics of pin-hole lenses; therefore, the proposed method can be applied to most DFP measurement systems equipped with pin-hole lenses. The Scheimpflug lens, commonly used in oblique measurement systems, cannot replace the proposed VFPYU method for addressing the DRI problem because the non-parallel light condition remains unchanged. It is noteworthy that there exist two exceptions. The first is when the distance between the lens and the object is very far and the field of view is very small so that the light rays can be regarded as almost parallel. But this condition is rare due to the low measurement accuracy; the second is when telecentric lenses are used for both the camera and projector, but the increase in hardware cost and structure size, as well as the limitation in measurement scenarios, need to be taken into consideration.

The proposed method yields accurate and reliable results within the pre-defined depth range. However, when the object to be measured is so large that it exceeds the depth range, the measurement will fail. Future research will concentrate on leveraging geometric constraints to enable robust phase unwrapping without depth range limitations, including post-processing such as learning-based methods to correct erroneous unwrapped phases, and combining spatial information or temporal information to improve fast and accurate 3-D measurements.

#### V. CONCLUSION

This article presents a VFPYU method for high-speed 3-D shape measurement. We demonstrate that the existing

geometric constraint-based phase unwrapping methods suffer from the DRI problem, causing unwrapping failure and measurement errors. To address this problem, we present an optimized variable-frequency fringe pattern. Unlike the traditional constant-frequency fringes, the proposed method theoretically determines the optimal fringe frequency according to the system's parameters and measurement depth range requirements. The encoding and decoding methods for the variable-frequency fringe patterns are detailed in this article.

Extensive experimental results demonstrate that the proposed VFPU method outperforms the widely used multi-frequency method, the phase-coding method, the Gray-code method, the misaligned Gray-code method, and the generalized Tri-PU method for higher measurement efficiency and accuracy. Furthermore, compared with the traditional geometric constraint methods, the proposed VFPU method effectively addresses the DRI problem and achieves higher measurement accuracy and robustness. Due to its high speed, high accuracy, and high robustness, the proposed method has significant advantages in high-speed 3-D measurement.

## REFERENCES

- [1] S. Zhang, "High-speed 3D shape measurement with structured light methods: A review," *Opt. Lasers Eng.*, vol. 106, pp. 119–131, Jul. 2018.
- [2] Y. Zheng et al., "A universal self-correcting approach for abnormal jump errors in absolute phase retrieval," *IEEE Trans. Instrum. Meas.*, vol. 71, pp. 1–13, 2022.
- [3] S. Lv and Q. Kemao, "Modeling the measurement precision of fringe projection profilometry," *Light, Sci. Appl.*, vol. 12, no. 1, p. 257, Oct. 2023.
- [4] J. Salvi, S. Fernandez, T. Pribanic, and X. Llado, "A state of the art in structured light patterns for surface profilometry," *Pattern Recognit.*, vol. 43, no. 8, pp. 2666–2680, Aug. 2010.
- [5] S. Feng, C. Zuo, W. Yin, G. Gu, and Q. Chen, "Micro deep learning profilometry for high-speed 3D surface imaging," *Opt. Lasers Eng.*, vol. 121, pp. 416–427, Oct. 2019.
- [6] S. Zhang, "Absolute phase retrieval methods for digital fringe projection profilometry: A review," *Opt. Lasers Eng.*, vol. 107, pp. 28–37, Aug. 2018.
- [7] X. Chen et al., "Two-digit phase-coding strategy for fringe projection profilometry," *IEEE Trans. Instrum. Meas.*, vol. 70, pp. 1–9, 2021.
- [8] H. An, Y. Cao, L. Wang, and B. Qin, "The absolute phase retrieval based on the rotation of phase-shifting sequence," *IEEE Trans. Instrum. Meas.*, vol. 71, pp. 1–10, 2022.
- [9] P. Zhou, Y. Cheng, J. Zhu, and J. Hu, "High-dynamic-range 3-D shape measurement with adaptive speckle projection through segmentation-based mapping," *IEEE Trans. Instrum. Meas.*, vol. 72, pp. 1–12, 2023.
- [10] R. M. Goldstein, H. A. Zebker, and C. L. Werner, "Satellite radar interferometry: Two-dimensional phase unwrapping," *Radio Sci.*, vol. 23, no. 4, pp. 713–720, Jul. 1988.
- [11] X. Su and W. Chen, "Reliability-guided phase unwrapping algorithm: A review," *Opt. Lasers Eng.*, vol. 42, no. 3, pp. 245–261, Sep. 2004.
- [12] T. J. Flynn, "Two-dimensional phase unwrapping with minimum weighted discontinuity," *J. Opt. Soc. Amer. A, Opt. Image Sci.*, vol. 14, no. 10, p. 2692, 1997.
- [13] X. He and Q. Kemao, "A comparison of n-ary simple code and n-ary gray code phase unwrapping in high-speed fringe projection profilometry," *Opt. Lasers Eng.*, vol. 128, May 2020, Art. no. 106046.
- [14] C. Zuo, L. Huang, M. Zhang, Q. Chen, and A. Asundi, "Temporal phase unwrapping algorithms for fringe projection profilometry: A comparative review," *Opt. Lasers Eng.*, vol. 85, pp. 84–103, Oct. 2016.
- [15] G. Sansoni, M. Carocci, and R. Rodella, "Three-dimensional vision based on a combination of gray-code and phase-shift light projection: Analysis and compensation of the systematic errors," *Appl. Opt.*, vol. 38, no. 31, p. 6565, 1999.
- [16] Z. Wu, W. Guo, and Q. Zhang, "Two-frequency phase-shifting method vs. Gray-coded-based method in dynamic fringe projection profilometry: A comparative review," *Opt. Lasers Eng.*, vol. 153, Jun. 2022, Art. no. 106995.
- [17] Y. Wang, K. Liu, Q. Hao, D. L. Lau, and L. G. Hassebrook, "Period coded phase shifting strategy for real-time 3-D structured light illumination," *IEEE Trans. Image Process.*, vol. 20, no. 11, pp. 3001–3013, Nov. 2011.
- [18] Y. Zhang, Z. Xiong, Z. Yang, and F. Wu, "Real-time scalable depth sensing with hybrid structured light illumination," *IEEE Trans. Image Process.*, vol. 23, no. 1, pp. 97–109, Jan. 2014.
- [19] J. Zeng et al., "Self-unwrapping phase-shifting for fast and accurate 3-D shape measurement," *IEEE Trans. Instrum. Meas.*, vol. 71, pp. 1–12, 2022.
- [20] Z. Li, K. Zhong, Y. F. Li, X. Zhou, and Y. Shi, "Multiview phase shifting: A full-resolution and high-speed 3D measurement framework for arbitrary shape dynamic objects," *Opt. Lett.*, vol. 38, no. 9, p. 1389, 2013.
- [21] W. Lohry, V. Chen, and S. Zhang, "Absolute three-dimensional shape measurement using coded fringe patterns without phase unwrapping or projector calibration," *Opt. Exp.*, vol. 22, no. 2, p. 1287, 2014.
- [22] G. E. Spoorthi, R. K. Sai Subrahmanyam Gorthi, and S. Gorthi, "PhaseNet 2.0: Phase unwrapping of noisy data based on deep learning approach," *IEEE Trans. Image Process.*, vol. 29, pp. 4862–4872, 2020.
- [23] S. Wang, T. Chen, M. Shi, D. Zhu, and J. Wang, "Single-frequency and accurate phase unwrapping method using deep learning," *Opt. Lasers Eng.*, vol. 162, Mar. 2023, Art. no. 107409.
- [24] A.-H. Nguyen, K. L. Ly, V. K. Lam, and Z. Wang, "Generalized fringe-to-phase framework for single-shot 3D reconstruction integrating structured light with deep learning," *Sensors*, vol. 23, no. 9, p. 4209, Apr. 2023.
- [25] C. Zuo et al., "Deep learning in optical metrology: A review," *Light, Sci. Appl.*, vol. 11, no. 1, p. 39, Feb. 2022.
- [26] Y. An, J.-S. Hyun, and S. Zhang, "Pixel-wise absolute phase unwrapping using geometric constraints of structured light system," *Opt. Exp.*, vol. 24, no. 16, p. 18445, 2016.
- [27] C. Jiang, B. Li, and S. Zhang, "Pixel-by-pixel absolute phase retrieval using three phase-shifted fringe patterns without markers," *Opt. Lasers Eng.*, vol. 91, pp. 232–241, Apr. 2017.
- [28] J. Dai, Y. An, and S. Zhang, "Absolute three-dimensional shape measurement with a known object," *Opt. Exp.*, vol. 25, no. 9, p. 10384, 2017.
- [29] Y. Wang, H. Xu, H. Zhu, X. Chen, and Y. Wang, "Pixel-wise phase unwrapping with adaptive reference phase estimation for 3-D shape measurement," *IEEE Trans. Instrum. Meas.*, vol. 72, pp. 1–9, 2023.
- [30] J. Yu and F. Da, "Absolute phase unwrapping for objects with large depth range," *IEEE Trans. Instrum. Meas.*, vol. 72, pp. 1–10, 2023.
- [31] T. Tao et al., "High-speed real-time 3D shape measurement based on adaptive depth constraint," *Opt. Exp.*, vol. 26, no. 17, p. 22440, 2018.
- [32] J.-S. Hyun and S. Zhang, "Enhanced two-frequency phase-shifting method," *Appl. Opt.*, vol. 55, no. 16, p. 4395, 2016.
- [33] H. Wu, Y. Cao, H. An, C. Xu, H. Li, and Y. Li, "A general phase ambiguity suppression algorithm combining geometric constraints and temporal phase unwrapping," *Opt. Laser Technol.*, vol. 150, Jun. 2022, Art. no. 107955.
- [34] J.-S. Hyun and S. Zhang, "Superfast 3D absolute shape measurement using five binary patterns," *Opt. Lasers Eng.*, vol. 90, pp. 217–224, Mar. 2017.
- [35] S. Lv, Q. Sun, Y. Zhang, J. Wang, and Y. Jiang, "Monotonicity analysis of absolute phase unwrapping by geometric constraint in a structured light system," *Opt. Exp.*, vol. 28, no. 7, p. 9885, 2020.
- [36] Z. Zhang, "A flexible new technique for camera calibration," *IEEE Trans. Pattern Anal. Mach. Intell.*, vol. 22, no. 11, pp. 1330–1334, May 2000.
- [37] P. S. Huang, "Novel method for structured light system calibration," *Opt. Eng.*, vol. 45, no. 8, Aug. 2006, Art. no. 083601.
- [38] H. Deng et al., "Direction-determined phase unwrapping using geometric constraints of the structured light system: The establishment of minimum phase map," *Opt. Commun.*, vol. 402, pp. 14–19, Nov. 2017.
- [39] Y. Wang and S. Zhang, "Novel phase-coding method for absolute phase retrieval," *Opt. Lett.*, vol. 37, no. 11, p. 2067, 2012.
- [40] L. Lu, Z. Wu, Q. Zhang, C. Chen, Y. Li, and F. Li, "High-efficiency dynamic three-dimensional shape measurement based on misaligned gray-code light," *Opt. Lasers Eng.*, vol. 150, Mar. 2022, Art. no. 106873.
- [41] Z. Wu, W. Guo, L. Lu, and Q. Zhang, "Generalized phase unwrapping method that avoids jump errors for fringe projection profilometry," *Opt. Exp.*, vol. 29, no. 17, p. 27181, 2021.
- [42] Z. Wu, C. Zuo, W. Guo, T. Tao, and Q. Zhang, "High-speed three-dimensional shape measurement based on cyclic complementary gray-code light," *Opt. Exp.*, vol. 27, no. 2, p. 1283, 2019.



**Jinghui Zeng** received the B.S. degree in optoelectronic information science and engineering from the South China University of Technology, Guangzhou, China, in 2017, where he is currently pursuing the Ph.D. degree in software engineering with the Shien-Ming Wu School of Intelligent Engineering.

His current research interests include computer vision, structured light 3-D measurement, and surface reconstruction.



**Yucheng Li** received the B.S. degree in measurement and control technology and instrument from Xiangtan University, Xiangtan, China, in 2017, and the M.S. degree in control science and engineering from Hunan University, Changsha, China, in 2020.

His current research interests include structured light, surface reconstruction, and high-performance computing.



**Chen Xu** received the Ph.D. degree in mechanical and electronic engineering from the South China University of Technology, Guangzhou, China, in 2009.

He is the President of Dongguan New Generation Artificial Intelligence Industry Technology Research Institute, Dongguan, China. His current research interests include LED lighting and 3-D measurement.



**Shutao Li** (Fellow, IEEE) received the B.S., M.S., and Ph.D. degrees in electrical engineering from Hunan University, Changsha, China, in 1995, 1997, and 2001, respectively.

In 2001, he joined the College of Electrical and Information Engineering, Hunan University, where he is currently a Full Professor. From May 2001 to October 2001, he was a Research Associate with the Department of Computer Science, The Hong Kong University of Science and Technology, Hong Kong. From November 2002 to November 2003, he was a Post-Doctoral Fellow with the Royal Holloway College, University of London, London, U.K. From April 2005 to June 2005, he was a Visiting Professor with the Department of Computer Science, The Hong Kong University of Science and Technology. He has authored or co-authored over 200 refereed articles. His research interests include image processing, pattern recognition, and artificial intelligence.

Dr. Li received the two Second-Grade State Scientific and Technological Progress Awards of China in 2004 and 2006.



**Mingkui Tan** (Member, IEEE) received the bachelor's degree in environmental science and engineering and the master's degree in control science and engineering from Hunan University, Changsha, China, in 2006 and 2009, respectively, and the Ph.D. degree in computer science from Nanyang Technological University, Singapore, in 2014.

From 2014 to 2016, he worked as a Senior Research Associate on computer vision with the School of Computer Science, The University of Adelaide, Adelaide, SA, Australia. He is currently a Professor with the School of Software Engineering, South China University of Technology, Guangzhou, China. His research interests include machine learning, sparse representation, large-scale optimization, and 3-D analysis.